JAVMA

AVMA®

Plasma and synovial fluid extracellular vesicles display altered microRNA profiles in horses with naturally occurring post-traumatic osteoarthritis: an exploratory study

Shannon S. Connard, DVM, DACVS[1,2]; Angela M. Gaesser, DVM, DACVS[3]; Emily J. Clarke, BSc, MRes, AFHEA, PhD[4]; Renata L. Linardi, DVM[3]; Kayla M. Even, BSc[3]; Julie B. Engiles, VMD, DACVP[3]; Drew W. Koch, DVM, PhD, DACVS[1,5]; Mandy J. Peffers, BSc, MPhil, PhD, BVetMed, FRCVS[4]; Kyla F. Ortved, DVM, PhD, DACVS, DACVSMR[3]*

[1]Department of Clinical Sciences, College of Veterinary Medicine and the Comparative Medicine Institute, North Carolina State University, Raleigh, NC
[2]Comparative Medicine Institute, North Carolina State University, Raleigh, NC
[3]Department of Clinical Studies, New Bolton Center, School of Veterinary Medicine, University of Pennsylvania, Philadelphia, PA
[4]Department of Musculoskeletal and Ageing Science, Institute of Life Course and Medical Sciences, University of Liverpool, Liverpool, United Kingdom
[5]Preclinical Surgical Research Laboratory, Department of Clinical Sciences, Colorado State University, Fort Collins, CO

*Corresponding author: Dr. Ortved (kortved@vet.upenn.edu)

OBJECTIVE
The objective of this study was to characterize extracellular vesicles (EVs) in plasma and synovial fluid obtained from horses with and without naturally occurring post-traumatic osteoarthritis (PTOA).

ANIMALS
EVs were isolated from plasma and synovial fluid from horses with (n = 6) and without (n = 6) PTOA.

METHODS
Plasma and synovial fluid EVs were characterized with respect to quantity, size, and surface markers. Small RNA sequencing was performed, and differentially expressed microRNAs (miRNAs) underwent bioinformatic analysis to identify putative targets and to explore potential associations with specific biological processes.

RESULTS
Plasma and synovial fluid samples from horses with PTOA had a significantly higher proportion of exosomes and a lower proportion of microvesicles compared to horses without PTOA. Small RNA sequencing revealed several differentially expressed miRNAs, including miR-144, miR-219-3p, and miR-199a-3l in plasma and miR-199a-3p, miR-214, and miR-9094 in synovial fluid EVs. Bioinformatics analysis of the differentially expressed miRNAs highlighted their potential role in fibrosis, differentiation of chondrocytes, apoptosis, and inflammation pathways in PTOA.

CLINICAL RELEVANCE
We have identified dynamic molecular changes in the small noncoding signatures of plasma and synovial fluid EVs in horses with naturally occurring PTOA. These findings could serve to identify promising biomarkers in the pathogenesis of PTOA, to facilitate the development of targeted therapies, and to aid in establishing appropriate translational models of PTOA.

Joint injury and cartilage damage are ubiquitous in equine athletes and pose a serious welfare problem in the equine industry.[1,2] If recognized early, joint injuries can often be treated with rest, rehabilitation, and targeted biotherapeutics to help decrease joint inflammation and promote articular tissue healing.[3,4] Unfortunately, joint trauma often goes unrecognized and precipitates post-traumatic osteoarthritis (PTOA), a degenerative, debilitating disease that is characterized by progressive degradation of the joint. Although complex cellular signaling and global articular inflammation are central in the development of PTOA, our understanding of the pathophysiology of PTOA remains incomplete. This knowledge gap

is evident in the lack of effective preventative and curative treatments, large financial burden, career-ending loss of athletic performance, decreased quality of life, and disease-associated mortalities.[5]

Constituting a rapidly expanding field of research, extracellular vesicles (EVs) have been identified to play a major role in both joint homeostasis and the pathophysiology of PTOA in humans and horses.[6,7] EVs are small, membrane-enclosed vesicles that are secreted by most mammalian cells. There are 3 sub-types of EVs that are classified based on their biogenesis and size as exosomes (approx 30 to 100 nm), microvesicles (approx 100 to 1,000 nm), and apoptotic vesicles (approx 1,000 to 5,000 nm). Exosomes are produced by the endosomal system and are the most biologically active, while microvesicles originate via outward budding of the plasma membrane, and apoptotic bodies are released by cells undergoing apoptosis. EVs carry biologic cargo consisting of nucleic acids, proteins, and lipids that change rapidly with disease.[6,8] MicroRNAs (miRNAs) make up the majority of the nucleic acids and play a critical role in intercellular communication, especially between chondrocytes and synoviocytes in the context of the joint.[9,10] Thus, EVs are ideal candidates to be used as biomarkers of early disease, cell-free biological therapies, and customizable delivery systems.

Significant differences have been characterized in the EV miRNA profile of plasma and synovial fluid obtained from humans and horses with and without osteoarthritis (OA).[11-13] In vitro studies have found that inflamed synoviocytes and chondrocytes produce EVs capable of rapidly and markedly upregulating proinflammatory cytokine cascades, including matrix metalloproteinases (MMPs) and aggrecanases, that degrade the extracellular matrix and decrease the biomechanical integrity of articular cartilage.[10] Several studies have characterized EV fatty acid signatures,[14] hyaluronic acid content,[15] and infrared spectra[16] in horses with naturally occurring OA; however, to the authors' knowledge, EV transcriptomes have only been characterized in equine models of induced OA.[12,13]

The present exploratory study aimed to characterize and perform transcriptomic profiling of plasma- and synovial fluid–derived EVs collected from horses with and without naturally occurring PTOA. We hypothesized that plasma and synovial fluid from horses with PTOA would contain EVs with significantly different subtypes and transcriptomes than horses without PTOA.

Methods

Horses and study design

The IACUC at The University of Pennsylvania (No. IACUC #806625) approved this study. All methods were conducted according to the national guidelines under which the institution operates and NIH Guidelines for the Care and Use of Laboratory Animals (8th edition). A total of 16 skeletally mature (greater than 2 years of age) Thoroughbred horses euthanized for reasons unrelated to this study were evaluated.

Based on the postmortem evaluation detailed in the subsequent methods, 12 euthanized horses with (n = 6) and without (n = 6) PTOA were included. All samples were obtained between January 2021 and June 2021. Plasma was collected before euthanasia, which was performed via pentobarbital sodium over-dose (140 mg/kg IV; Vortech). Immediately following euthanasia, synovial fluid samples were obtained from the radiocarpal, middle carpal, and metacarpophalangeal joints as detailed below.

Plasma and synovial fluid sampling

Plasma was collected premortem via venipuncture following aseptic preparation of the jugular vein. Samples were collected directly into EDTA tubes (BD Vacutainer; BD A/S). Synovial fluid samples were obtained at random from either the right or left radiocarpal, middle carpal, and metacarpophalangeal joints. Synovial fluid was aspirated aseptically using an 18-gauge, 38.1-mm needle, transferred into EDTA tubes, and gently inverted 5 to 10 times. All biofluids were temporarily stored on ice and processed within 1 hour of collection. Plasma samples were centrifuged at 3,000 X g for 15 minutes at 4 °C. Synovial fluid underwent cell removal by centrifugation at 2,700 X g for 30 minutes at room temperature. Plasma and cell-free synovial fluid samples were stored at –80 °C.

Postmortem examination

Following euthanasia, the radiocarpal, middle carpal, and metacarpophalangeal joints that had undergone arthrocentesis were grossly examined and graded for OA based on a modified Osteoarthritis Research Society International (OARSI) scoring system for equine joints[17] by a board-certified pathologist (JBE). **Supplementary Table S1** summarizes the macroscopic articular cartilage staging used to assign erosion scores to the radiocarpal and middle carpal joints in addition to wear line, erosion, and palmar arthroses grades to metacarpophalangeal joints. Following gross examination, horses were selected and grouped based on modified OARSI scores of PTOA severity, resulting in a total of 6 control joints (modified OARSI scores of 0) and 6 joints with advanced PTOA (modified OARSI scores averaging ≥ 2 for metacarpophalangeal joints or ≥ 3 for middle carpal and radiocarpal joints).

EV isolation

Cell-free synovial fluid samples were treated with 10 µg/mL hyaluronidase (from bovine testes; Sigma-Aldrich) for 30 minutes at room temperature on a rotor with constant agitation. Protein aggregates were removed by centrifugation at 3,000 X g for 5 minutes at room temperature in an Eppendorf centrifuge (Hettich Mikro 200R with rotor 2424A). The supernatants were transferred into SW60 tubes (Beckman Coulter) and gently mixed with 2 mL PBS. Plasma and hyaluronidase-treated synovial fluid EVs were subsequently isolated by ultracentrifugation as previously described.[18] Briefly, EVs were pelleted with 3 sequential ultracentrifugation

steps of 15,000 X *g* for 30 minutes and 100,000 X *g* for 90 minutes to pellet the EVs, after which they were resuspended in PBS and centrifuged again at 100,000 X *g* for 90 minutes using a SW60-Ti rotor in a Beckman Coulter Optima™ ultracentrifuge at 48 °C. Final EV pellets were resuspended in 100 µL PBS.

EV characterization

Nanoparticle tracking analysis—A ZetaView nanoparticle tracking analyzer (NTA; Particle Metrix) together with ZetaView 8.05.12 SP2 software were utilized to determine size distribution and particle concentration. Prior to analysis, the instrument was calibrated with 100-nm polystyrene nano standard particles. For all the samples, 10 µL of isolated EVs were diluted to 1:500 to 1:8,000 in particle-free 1X PBS. Each sample was loaded, and cell quality and particle drift were assessed prior to capturing the video. The video was captured at a sensitivity of 75, a shutter speed of 75, and a frame rate of 30 frames/seconds. The samples were read at 11 positions for 3 cycles to determine the size (in nm) and concentration (in particles per mL). EV size distribution data was sorted to quantify the 3 EV subtypes based on size—exosomes (0 to 99 nm), microvesicles (100 to 1,000 nm), and apoptotic bodies (1,001 to 6,000 nm). The proportion of each subtype was then calculated by dividing the number of EVs in each category by the total number of EVs counted.

Western blot—EV samples (1 X 10⁹ particles) containing 2X Laemmli loading buffer were loaded into a 4% to 12% precasted gel in a nonreducing condition. Precision Plus Protein Kaleidoscope Prestained Protein Standards and PageRuler Prestained Protein Ladder were used as molecular weight markers. The electrophoresis was initially run at 80 V for 20 minutes and then at 150 V for 60 minutes. The proteins were transferred from the gel to a polyvinylidene difluoride membrane at 70 V for 2 hours. After transfer, the membrane was briefly rinsed in Tris-buffered saline solution and blocked with 5% dry skim milk for 2 hours at room temperature before incubation with a primary antibody overnight at 4 °C. Primary antibodies included anti-CD9, anti-CD81, anti-TSG101, and anti-calnexin. Then, the membrane was washed with Tris-buffered saline plus Tween 20 at room temperature (3 times for 5 minutes each) and then incubated with horseradish peroxidase–conjugated secondary antibody for 1 hour at room temperature. Secondary antibodies included goat anti-mouse for CD9 and CD81 and donkey anti-rabbit for TSG101. The membrane was washed with Tris-buffered saline plus Tween 20 for 2 hours, changing the wash every 15 to 20 minutes, and then incubated with Immobilon Forte Western HRP Substrate for 2 minutes at room temperature for chemiluminescence detection. Detection was performed with Cytiva Amersham ImageQuant 800 with 30 to 120 seconds of exposure time.

Transmission electron microscopy—A 5-µL volume of sample was applied to a thin carbon-coated copper grid that was glow discharged for 2 minutes using a Pelco Easyglow instrument. Then, 5 µL of freshly made 2% uranyl acetate stain solution was applied to the sample holding grid and incubated for 2 minutes on the grid. Excess sample and stain were blotted away with a Whatman filter paper, leaving a thin layer of stained particles on the grid. The staining and blotting process was repeated with 2% uranyl acetate, and the grid was left to dry until imaged. Transmission electron microscopy (TEM) micrographs were collected using a Tecnai T12 TEM microscope at 100 keV. The images were recorded on a Gatan Oneview 4K X 4K camera. Each image was collected by exposing the sample for 4 seconds, and a total of 100 dose-fractionated images were collected and averaged into a high-resolution motion-corrected micrograph. The data was collected at –1.5 to 2 µm under focus and at 30K magnification. Fifteen microscopic fields were observed, and representative images were selected.

Small RNA sequencing

RNA extraction—Total RNA, including small RNAs (sRNAs), was purified from plasma and synovial fluid EVs using the Quick-RNA Miniprep Kit (Zymo Research Corporation). The RNA isolated from the EVs was analyzed using an Agilent 2100 Bioanalyzer and an RNA 6000 Pico kit (Agilent Technologies) to determine RNA concentration, purity, and integrity. The RNA amount was represented by total RNA measured. RNA samples were stored at –80 °C.

sRNA sequencing—Due to low concentrations of RNA isolated from EVs, samples from the 6 horses within each group were pooled (control [n = 1] and PTOA [n = 1]) and shipped according to company protocols to GENEWIZ, a division of Azenta Life Sciences, for sRNA sequencing. Library preparation included ligation of sequencing adapters to 5′ phosphate ends. The RNA fragments were then converted to cDNA libraries prior to sequencing to target sRNA products of 18 to 30 basepairs. Briefly, raw reads obtained from miRNA sequencing were processed by removing contamination and adapter sequences. Statistical analysis on lengths and counts of the filtered reads as well as data volume was performed as part of data quality control. The filtered reads were aligned to the miRbase database, composed of known miRNA sequences, and followed by miRNA annotation. Additionally, the reads were aligned to the Rfam database to study noncoding RNA distribution. For novel miRNA prediction, the sequences were aligned to the *Equus caballus* genome and subject to RNA folding and secondary structure analysis. miRNA differential expression (DE), clustering, and target gene prediction were also analyzed. The original image data were analyzed using Bcl2fastq for base calling and preliminary quality analysis. During the sequencing process, the quality of the first 25 bases of each read determined whether the read was retained or discarded via Illumina built-in software. Trimmomatic v0.30 was used to process the raw data to clean data for subsequent data analysis. Noncoding RNAs were classified and annotated by aligning clean reads to

3

the Rfam database using BLASTN. The best query-reference match was used as the alignment result. To remove the repetitive sequences in the sRNAs, the sRNA sequences were aligned to the repetitive sequence reference of the given species or predicted based on the sequence of the reference *E caballus* genome. The miRNA sequences were aligned to mRNA exons and introns to identify the original mRNA of the miRNA fragment. miRNA prediction was performed by aligning the reads to the reference genome, then utilizing miRDeep2 V2.0.0.7 to model all the possible secondary structures of miRNA precursors based on the alignment information. The secondary structures were then subject to a scoring system for evaluation to determine the novel miRNA sequence. miRNA family classification was then performed on the annotated known miRNAs to explore the presence of the miRNA family in other species. Miranda v3.3a was used to predict target sites based on miRNA sequences and the corresponding genomic cDNA sequences.

Statistical analysis

EV characterization—Data were assessed for normality by visual inspection of histograms followed by a Shapiro-Wilk test. Nonparametric data are reported as median (range). Continuous parametric data, including horse age and NTA EV diameter are presented as mean ± SD. Horse age was analyzed using an unpaired *t* test. A mixed-effects model, with horse as a random effect, was used for the comparison of all quantitative outcome variables between treatment groups. All analyses were performed using JMP Pro 17 and GraphPad Prism version 10.1.0 (GraphPad Software Inc). Significant differences between the groups were identified at $P < .05$.

DE miRNA—The miRNA expression was analyzed in clusters to examine the differences across all miRNAs within the same cluster. The read count from the miRNA expression analysis was used as the input for this analysis. DE miRNAs were analyzed using DESeq2 V1.16.1. Due to the use of a single pooled sample for each group (control [n = 1] and PTOA [n = 1]) containing EVs from 6 horses, statistical analysis could not be performed; however, each sample was treated as a replicate for the estimation of dispersion. DE miRNAs were identified based on the criteria of fold change > 2 between groups (control and PTOA) in order to explore the upregulated and downregulated genes.

Functional enrichment analysis—Ingenuity Pathway Analysis (IPA; Qiagen) "Core Analysis" was used to identify potential biological associations of plasma and synovial fluid EV DE miRNAs using *P* values. For network generation, default settings were used to identify miRNAs whose expression was differentially regulated. These molecules were overlaid onto a global molecular network contained in the Ingenuity Knowledge Base. Networks of "network-eligible molecules" were then algorithmically generated based on their connectivity. The functional analysis identified the biological functions and diseases that were most significant to the data set. A right-tailed Fisher's exact test was used to calculate *P* values. Canonical pathway analysis identified the pathways from the IPA library that were most significant to the data set. Analysis was performed on all transcriptomics data, comparing control and PTOA cohorts, and the MicroRNA Target Filter module within IPA was used to identify putative mRNA targets. A conservative filter of "experimentally validated" mRNA targets was used for each miRNA. Networks were prioritized based on their consistency score, which does not measure statistical significance but identifies relationships in node expression that are observed or predicted based on findings from the Ingenuity Knowledge Base. ToppGene was used for functional enrichment analysis of the miRNA targets.[19] Biological process gene ontology terms generated through ToppGene were then summarized, and REViGO[20] and Cytoscape[21] were used to visualize the network.

Results

Donor cohorts

A total of 12 Thoroughbred horses without (n = 6) and with advanced PTOA (n = 6) were selected based on modified OARSI scores of PTOA severity **(Figure 1)**. Control joints included radiocarpal (n = 2), middle carpal (n = 2), and metacarpophalangeal (n = 2). PTOA joints were comprised of radiocarpal (n = 1; OARSI score, 4), middle carpal (n = 3; median OARSI score, 3; range, 3 to 4), and metacarpophalangeal (n = 2; median wear line score, 3; range, 3 to 3; median erosion score, 2; range, 2 to 2; and median palmar arthroses score, 1.5; range, 1 to 2). The ages of the healthy cohort (4 ± 1.53 years) and PTOA cohort (7 ± 1.91 years) were significantly different ($P < .05$). The summary of all donors' information is provided **(Table 1)**.

EV characterization

The concentration of EVs and particle size distribution were determined by NTA. No significant differences were identified in the concentration of plasma or synovial fluid EV between control and PTOA horses **(Figure 2)**. The mean (± SD) particle diameter for plasma EVs from control horses and horses with PTOA was 150.68 ± 15.27 nm and 121.93 ± 18.97 nm, respectively. The mean synovial fluid EV particle diameter was 160.32 ± 7.96 nm from control joints and 137.88 ± 25.43 nm from joints with PTOA. The mean concentration of exosomes, microvesicles, and apoptotic bodies was calculated. In both plasma and synovial fluid EVs from horses with PTOA, there was a significant increase in the proportion of exosomes and decrease in the proportion of microvesicles compared to healthy horses (Figure 2). Western blot was performed to confirm the presence of specific EV markers, including CD9, CD81, and TSG-101. Additionally, calnexin immunoblotting was included as a negative control to demonstrate that isolated EVs were pure, enriched vesicles. The expression of the transmembrane tetraspanin proteins CD9 and
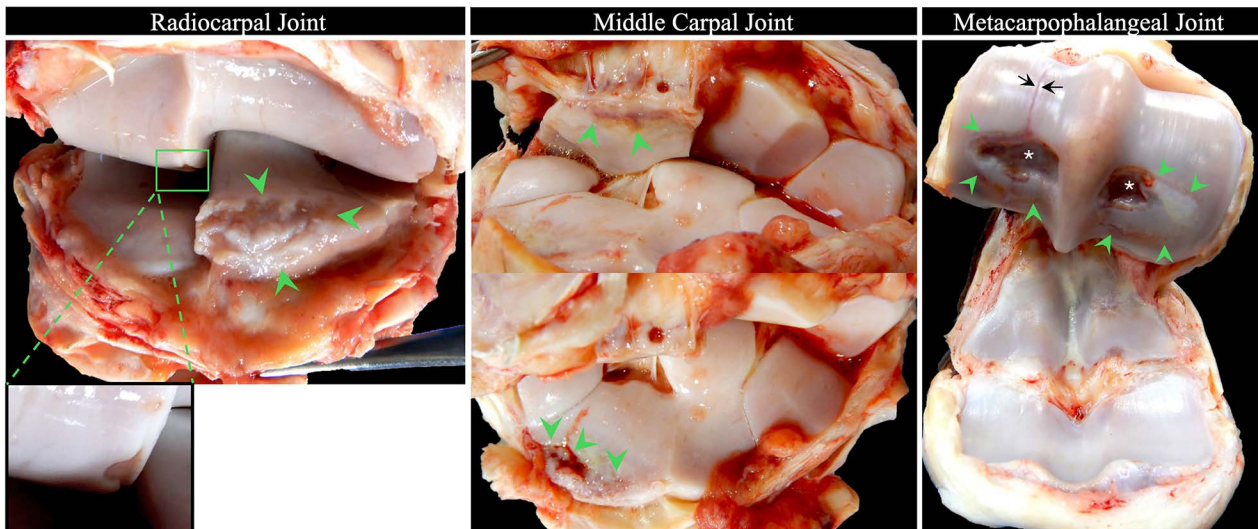
Figure 1—Representative images from radiocarpal, middle carpal, and metacarpophalangeal joints classified as advanced post-traumatic osteoarthritis (PTOA) based on the modified Osteoarthritis Research Society International scores/grades for articular cartilage erosions (green arrowheads, green box), wear lines (black arrows), and palmar arthroses of the third metacarpal condyles (white asterisks).

Table 1—Donor information for control and post-traumatic osteoarthritis (PTOA) samples.

Cohort	Sample	Age (y)	Breed	Sex	Joint	Modified OARSI score
Control	1	3	Thoroughbred	Filly	Left middle carpal	0
	2	3	Thoroughbred	Filly	Left radiocarpal	0
	3	4	Thoroughbred	Mare	Left radiocarpal	0
	4	2	Thoroughbred	Gelding	Left metacarpophalangeal	0, 0, 0
	5	6	Thoroughbred	Gelding	Left metacarpophalangeal	0, 0, 0
	6	6	Thoroughbred	Gelding	Left middle carpal	0
PTOA	1	5	Thoroughbred	Mare	Left middle carpal	4
	2	10	Thoroughbred	Mare	Right metacarpophalangeal	3, 2, 2
	3	5	Thoroughbred	Gelding	Left middle carpal	3
	4	6	Thoroughbred	Gelding	Left metacarpophalangeal	3, 2, 1
	5	7	Thoroughbred	Gelding	Right middle carpal	3
	6	9	Thoroughbred	Gelding	Left radiocarpal	4

Modified Osteoarthritis Research Society International (OARSI) score presented as wear line, erosion, and palmar arthrosis scores (0 to 3) for metacarpophalangeal joints and erosion score (0 to 4) for middle carpal and radiocarpal joints as defined in the table.

CD81 and the endosomal protein TSG101, in addition to the absence of calnexin, were observed in all samples (Figure 2). The morphology of isolated EVs was investigated by TEM. Ultrastructural assessment of isolated EVs revealed the expected size distribution and membrane integrity. A heterogeneous population of EVs was detected, corroborating results from the NTA analysis. Most EVs were spherical, while some were heterogeneous in shape (Figure 2).

sRNA sequencing results

A total of 658 DE miRNAs, 67 known and 591 novel, were identified in plasma EVs from control horses and horses with PTOA. When investigating synovial fluid EVs from control and PTOA joints, there were 805 DE miRNAs, including 74 known and 731 novel **(Supplementary Table S2)**. The most DE miRNAs from both cohorts are shown **(Table 2)**.

There were 20 DE miRNAs (miR-19a, miR-29c, miR-132, miR-144, miR-183, miR-185, miR-194, miR-195, miR-199a-3p, miR-200a, miR-200b, miR-219-3p, miR-409-3p, miR-411, miR-499-5p, miR-628a, miR-1301, miR-3200, miR-7177b, and miR-9055) in both plasma and synovial fluid EVs. Data presented in this study are available using National Center for Biotechnology Information (NCBI) Gene Expression Omnibus (GEO); accession GSE256340. The datasets supporting the conclusions of this article are included within the article and its supplementary materials.

Bioinformatics analysis of DE miRNAs in plasma and synovial fluid

Pathway analysis of DE miRNAs—The 67 known plasma EV DE miRNAs were input into IPA "Core Analysis," yielding 38 mapped and 29 unmapped DE miRNAs. There were 9 duplicates within the
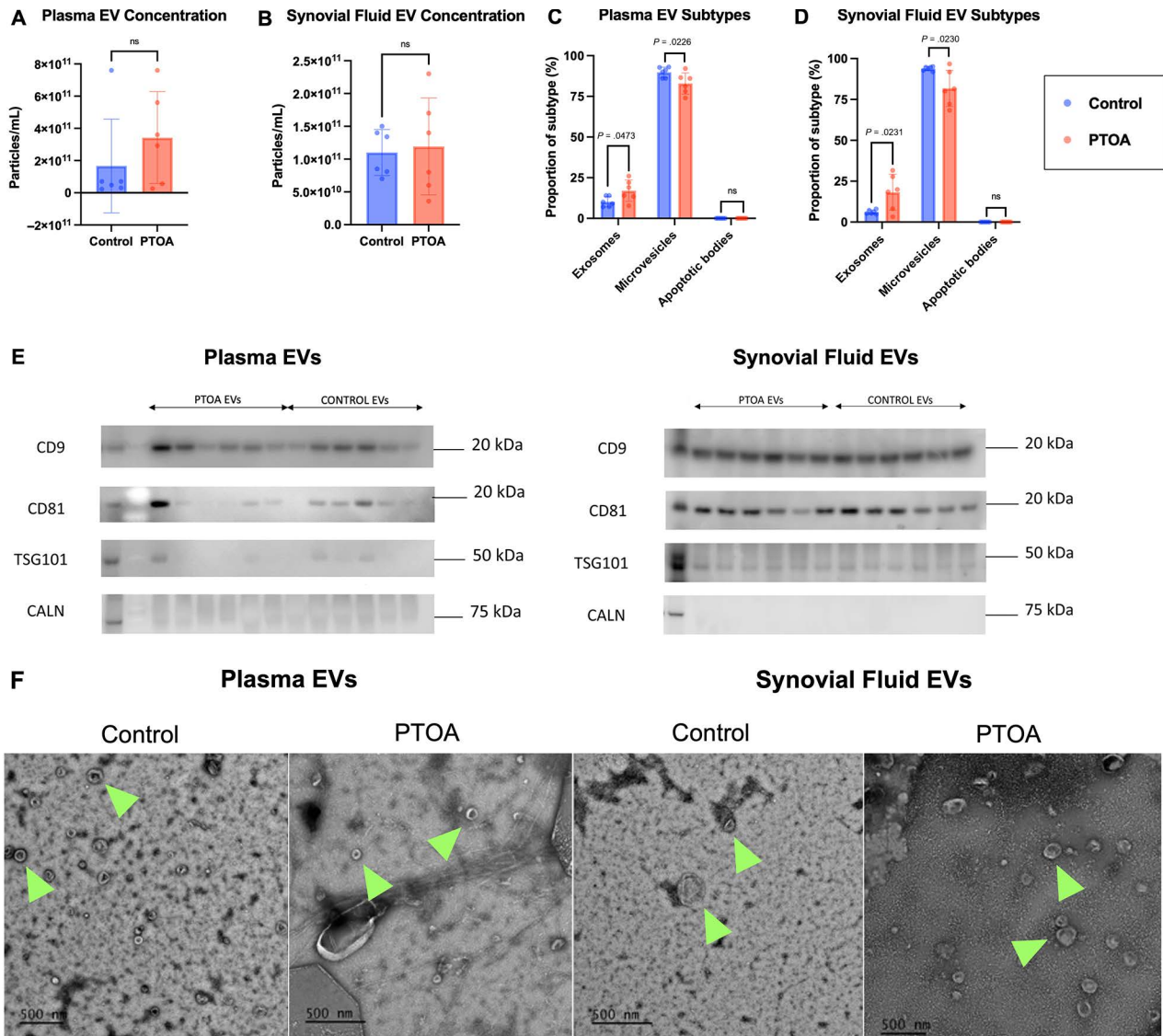
5

Figure 2—Nanoparticle tracking analysis, western blot, and transmission electron microscopy characterization of extracellular vesicles (EVs) from plasma and synovial fluid obtained from horses without (control) and with PTOA. Nanoparticle tracking analysis EV concentration and subtype data were evaluated using a mixed-effects model with horse as a random effect. There was no significant (ns) difference between plasma (A) or synovial fluid (B) EV concentration between control horses and horses with PTOA. There was a significant increase in plasma (C) and synovial fluid (D) exosomes in horses with PTOA compared to control and a significant decrease in plasma (C) and synovial fluid (D) microvesicles in horses with PTOA compared to control. (E) Western blot analysis of specific EV surface markers using antibodies CD9, CD81, TSG101, and calnexin confirmed the expression of CD9, CD81, and TSG101 and the absence of calnexin. (F) Transmission electron microscopy characterization of EVs isolated from plasma and synovial fluid detected a heterogeneous population of EVs (green arrowheads). Ultrastructural assessment confirmed expected EV size distribution and membrane integrity.

38 mapped DE miRNAs, resulting in 33 analysis-ready molecules across observations. Of these 33 DE miRNAs, 10 were downregulated and 23 were upregulated. IPA identified the top diseases and functions using activated Z-scores, which deduce the activation states of biological functions based on comparison with a model that assigns random regulation directions; negative Z-scores predict inhibition, while positive Z-scores predict activation. Top diseases and functions included inhibition of cellular development (Z-score, −2.133), cell-to-cell signaling and interaction (Z-score, −2.105), organismal injury and abnormalities (Z-score, −1.992), activation of cellular migration (Z-score, 2.312), differentiation of mesenchymal stem cells (Z-score, 2.000), and cell proliferation (Z-score, 1.982). Cellular functions pertinent to the pathophysiology of PTOA comprised of differentiation of mesenchymal stem cells, fibrosis, inflammation, migration of fibroblasts, and proliferation of chondrocytes were used to build the pathway **(Figure 3)**. The top scoring network identified was "Cellular Movement, Gene Expression" (score 60), which was expanded with OA-related canonical pathways **(Supplementary Figure S1)**.

Table 2—Differentially expressed plasma and synovial fluid extracellular vesicle microRNAs (miRNAs) with the highest and lowest log2 fold change when comparing horses with PTOA to control horses.

Plasma miRNAs	LogFC	Synovial fluid miRNAs	LogFC
Upregulated plasma miRNAs in PTOA		**Upregulated synovial fluid miRNAs in PTOA**	
eca-miR-144	13.6237682	eca-miR-199a-3p	19.5075097
eca-miR-502-3p	12.5897438	eca-miR-9094	11.6038972
eca-miR-3200	10.4806726	eca-miR-342-3p	10.8280809
eca-miR-185	10.0920876	eca-miR-615-3p	10.8280809
eca-miR-9179	10.0517109	eca-miR-3200	10.7439475
eca-miR-9126	9.92332278	eca-miR-187	10.4723927
eca-miR-491-5p	9.83090904	eca-miR-184	9.98886477
eca-miR-190b	9.59278891	eca-miR-144	9.95718746
eca-miR-9177	9.33462253	eca-miR-490-3p	9.95718746
eca-miR-450b-5p	9.25149976	eca-miR-9151	9.79940301
Downregulated plasma miRNAs in PTOA		**Downregulated synovial fluid miRNAs in PTOA**	
eca-miR-219-3p	−12.794912	eca-miR-214	−13.598883
eca-miR-199a-3p	−12.383964	eca-miR-345-3p	−10.840327
eca-miR-660	−12.354757	eca-miR-194	−10.4995
eca-miR-29c	−11.393837	eca-miR-29c	−10.166859
eca-miR-3548	−10.098001	eca-miR-628a	−10.110766
eca-miR-425	−9.8784364	eca-miR-15a	−10.052403
eca-miR-381	−9.5973535	eca-miR-379	−9.9280783
eca-miR-383	−7.3891094	eca-miR-9060	−9.2007238
eca-miR-149	−7.138274	eca-miR-483	−9.1120702
eca-miR-211	−4.0869879	eca-miR-105	−8.8632026

The 74 known synovial fluid EV DE miRNAs were processed using the same IPA "Core Analysis." There were 50 mapped and 24 unmapped DE miRNAs, including 4 duplicates, conceding 43 analysis-ready molecules across observations. Of these, 21 were downregulated and 22 were upregulated. Top diseases and functions encompassed inhibition of apoptosis (Z-score, −2.200), cell death (Z-score, −1.979), and senescence (Z-score, −1.960) and activation of expression of RNA (Z-score, 2.506), cell proliferation (Z-score, 2.347), cell viability (Z-score, 2.186), angiogenesis (Z-score, 2.049), stem cell proliferation (Z-score, 2.000), and cell proliferation of fibroblasts (Z-score, 1.980). The pathway was expanded with cellular functions pertinent to the pathophysiology of PTOA, including angiogenesis, cell viability, differentiation of bone cells, differentiation of stem cells, fibrosis, inflammation, and proliferation of chondrocytes (Figure 3). The top scoring network was "Gene Expression, Organismal Injury and Abnormalities" (score 57), which was expanded using OA-related canonical pathways (Supplementary Figure S1).

Pathway analysis of DE miRNA-predicted target genes—Further pathway analysis was performed using IPA Target Filter to investigate the position of the DE miRNA expression networks by integrating computational algorithms with multiple miRNA databases. We used a highly conservative threshold of "experimentally validated" in addition to filtering for tissue (cartilage) and cell lines (chondrocytes, fibroblasts, macrophages/monocytes, mesenchymal stem cells, and osteoblasts) pertinent to joint homeostasis and OA pathogenesis. This isolated 37 plasma EV miRNAs targeting 602 mRNAs **(Supplementary Table S3)** and 36 synovial fluid EV miRNAs with 596 mRNA targets **(Supplementary**

Table S4). The combined DE miRNAs and target mRNAs for plasma and synovial fluid were input separately into IPA "Core Analysis," and all the results for plasma and synovial fluid EVs are summarized in Supplementary Tables S3 and S4, respectively. Top canonical pathways are detailed in **Supplementary Table S5**, with high molecule involvement in the hepatic fibrosis, wound healing, senescence, and OA pathways. The main mRNA upstream regulators overlapping in both plasma and synovial fluid included miR-16-5p, miR29b-3p, and transforming growth factor β (TGFβ) (Supplementary Table S5). The top networks identified for plasma and synovial fluid EV DE miRNA target mRNAs are provided in Supplementary Tables S3 and S4, respectively.

The plasma EV combined DE miRNAs and target mRNAs top network, "Cellular Function and Maintenance, Gene Expression, Protein Synthesis" (score 36), was overlaid with germane biological processes, including adhesion of bone, development of fibroblast cell lines, expansion of chondrocyte layer, fibrosis, and regulation of osteoblasts **(Supplementary Figure S2)**. The network "Connective Tissue Disorders, Inflammatory Disease, Inflammatory Response" (score 22) shows pertinent biological processes, including organization of angiogenesis, bone lesion, fibrosis, inflammation of the joint, organization of collagen fibrils, OA, and rheumatoid arthritis, which were linked to relevant canonical pathways (Supplementary Figure S2). The top networks for synovial fluid EV combined DE miRNAs and target mRNAs included "Cellular Development, Cellular Growth and Proliferation, Connective Tissue Development and Function" (score 59) and "Cell Death and Survival, Cellular Movement, and Gene Expression" (score 46). The "Cellular Development, Cellular Growth and Proliferation, Connective Tissue
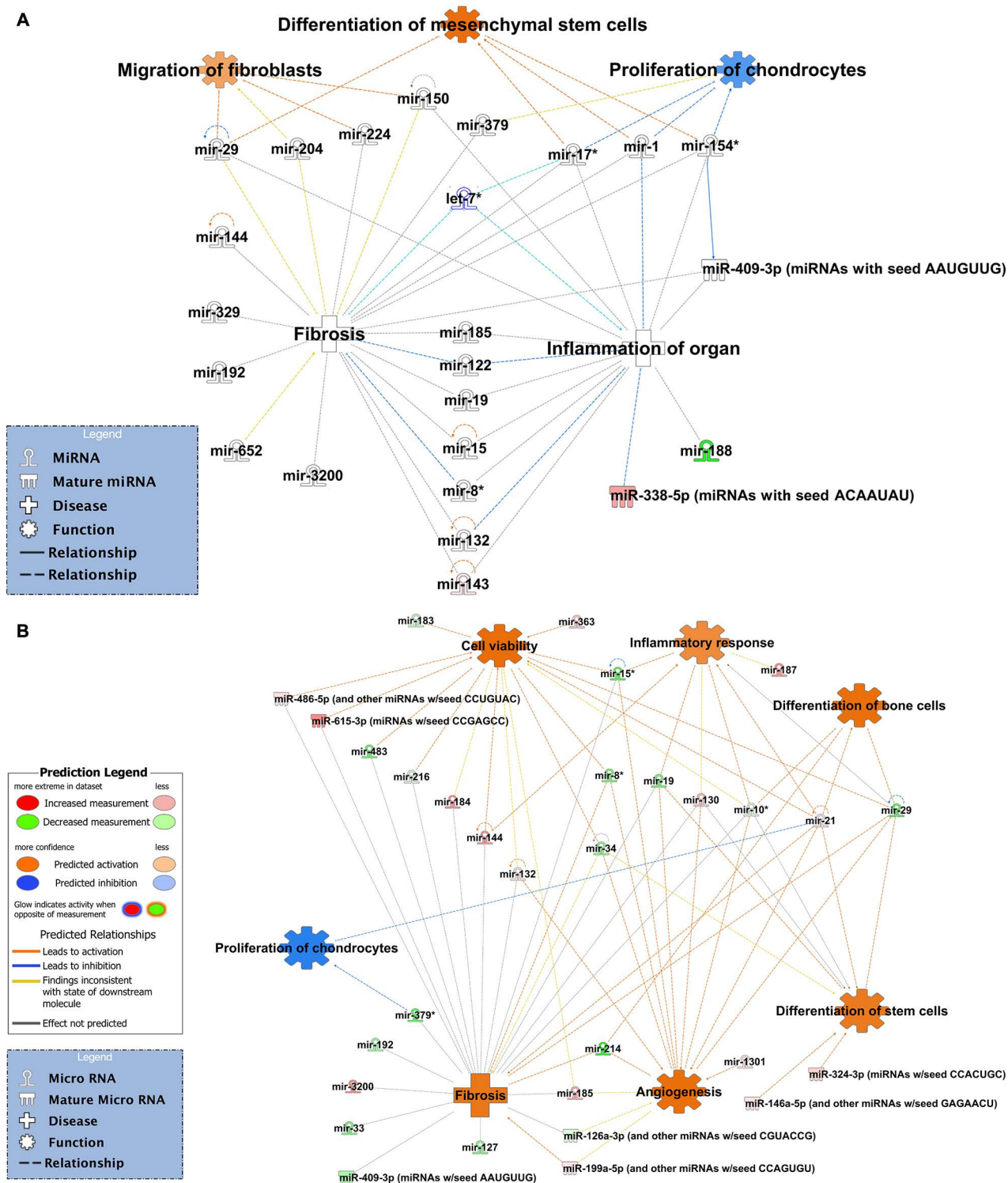
7

Figure 3—Ingenuity Pathway Analysis (IPA)-derived functions of differentially expressed (DE) plasma EV microRNAs (miRNAs). A—IPA cellular functions, including fibrosis, differentiation of mesenchymal stem cells, proliferation of chondrocytes, and inflammation, were correlated with plasma EV DE miRNAs. B—Synovial fluid DE miRNAs were associated with IPA cellular functions, including fibrosis, differentiation of mesenchymal stem cells, differentiation of chondrocytes, cell viability, angiogenesis, and inflammation. Figures generated are graphical representations of molecules identified in our data in their respective networks. Molecule color indicates upregulation (red) or down-regulation (green). Cellular function color denotes predicted activation (orange), inhibition (blue), or those which could not be predicted (gray) in PTOA. Intensity of color is directly proportionate to fold change. Legends to the main features in the networks are shown. Scale bar, 500 nm.
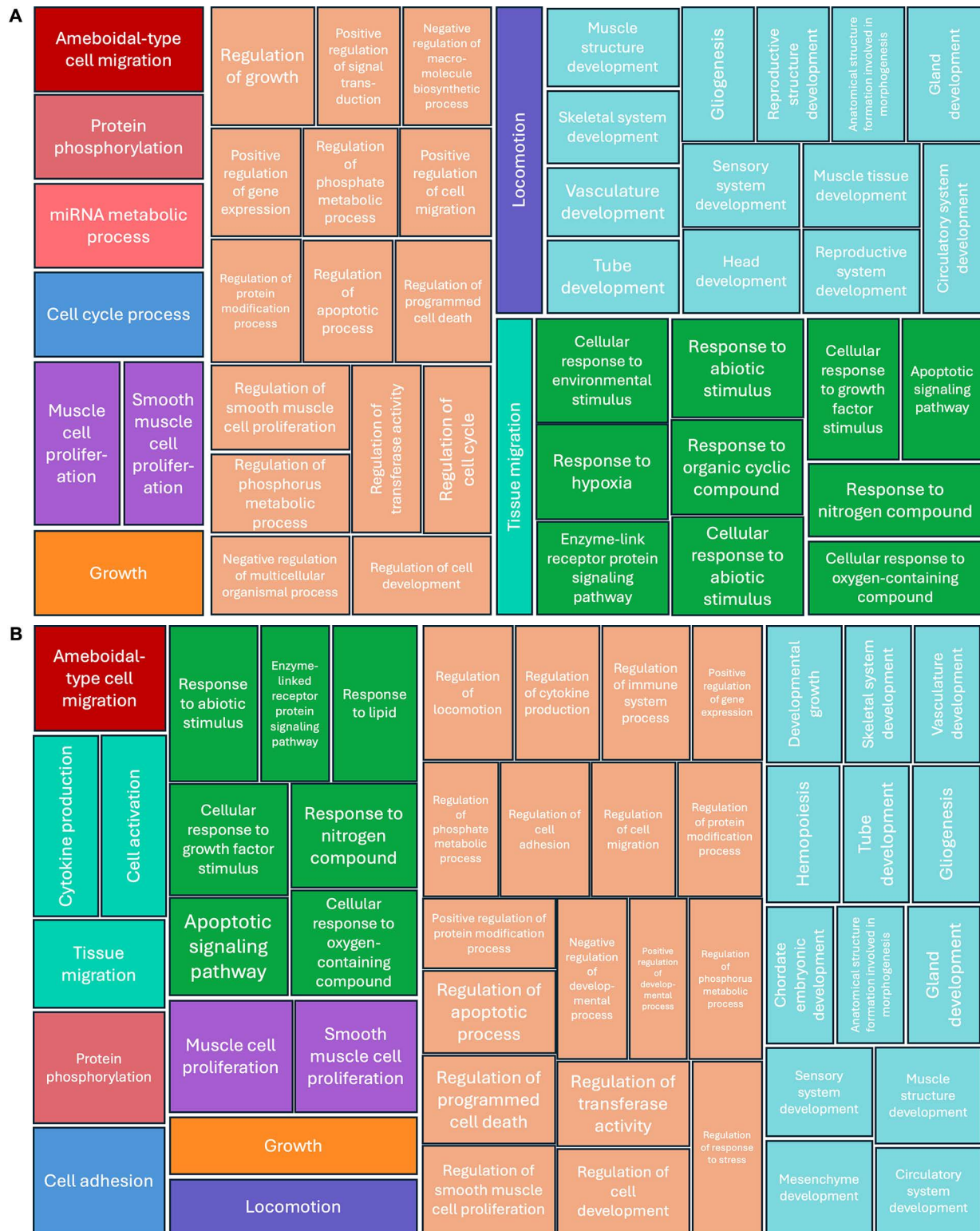
8

Figure 4—Bioinformatics analysis of plasma (A) and synovial fluid (B) EV DE miRNAs following small RNA sequencing and their putative mRNA targets. Treemap of the top 100 gene ontology (GO) terms. Hierarchical level is represented by a different colored rectangle (branch), each containing smaller rectangles (leaves). The size of the space inside each rectangle is based on the measured value. GO biological processes associated with dysregulated mRNA targets were identified following the TargetScan filter module in IPA. ToppGene was used to perform a functional enrichment analysis of predicted miRNA targets to highlight biological processes most significantly affected by dysregulated miRNA-mRNA interactions. GO terms (false discovery rate < 0.05) were summarized and visualized using REViGO and Cytoscape. The allowed similarity setting in REViGO is medium. Boxes represent the top biological processes that were significantly influenced by dysregulated miRNAs between horses with and without PTOA.

Development and Function" network was overlaid with germane biological processes, including condensation of cartilage tissue, cell death of connective tissue cells, differentiation of mesenchymal stem cells, expansion of chondrocyte layer, generation of mRNA, organismal death, and regulation of osteoblasts **(Supplementary Figure S3)**. The network "Cell Death and Survival, Cellular Movement, and Gene Expression" encompassed key biological processes, including angiogenesis, apoptosis, cell proliferation of fibroblasts, differentiation of bone, differentiation of osteoblasts, differentiation of osteoclasts, fibrosis, and inflammation of organ, which were linked to relevant canonical pathways (Supplementary Figure S3).

The putative target mRNAs were input into the gene ontology tool ToppGene. Analyses for both plasma and synovial fluid **(Supplementary Table S6)** EV DE miRNA putative target mRNAs identified "regulation of programmed cell death" and "regulation of apoptotic process" as top biological processes. The biological processes for each group were visualized using REViGO and Cytoscape. The top 100 biological processes for plasma and synovial fluid EV DE miRNA putative target mRNAs were categorized in Treemap **(Figure 4)**.

Discussion

As the characterization and understanding of EV involvement in the pathogenesis of PTOA evolves, it facilitates the identification of novel molecules that can be used to detect early pathology and/or that can be pursued as therapeutic targets. Several studies have shed light on the intricate role EVs isolated from plasma and synovial fluid play in both humans and horses affected by PTOA. To our knowledge, this is the first study in which both plasma- and synovial fluid–derived EVs have been characterized and undergone unbiased transcriptome profiling in horses with naturally occurring PTOA.

EVs were isolated from plasma and synovial fluid obtained from control horses and horses with advanced PTOA. The isolated plasma and synovial fluid EVs constituted a heterogenous population. Plasma EVs may have originated from any cell with access to peripheral vasculature, while synovial fluid EVs were likely derived from both plasma, as synovial fluid is an ultrafiltrate of plasma, and local cells found in the intra-articular environment, including synoviocytes and chondrocytes. Our NTA mean EV diameter (plasma control, 151 nm; plasma PTOA, 122 nm; synovial fluid control, 160 nm; and synovial fluid PTOA, 138 nm) were comparable to other plasma[13,22] and SF[11,13] studies (approx 100 nm) that used similar EV isolation methods. Interestingly, human plasma EVs isolated using EV precipitation and nanoparticle tracking methods from patients with OA[23] had a larger mean diameter size (235 nm) compared to the equine plasma EVs in our study (plasma control, 151 nm; plasma PTOA, 122 nm), which could be attributed to differences in EV isolation techniques. NTA found no significant difference in the concentration of EVs isolated from plasma

or synovial fluid samples from horses with or without PTOA. However, both plasma and synovial fluid samples from horses with PTOA had a significantly higher proportion of exosomes and a lower proportion of microvesicles compared to healthy horses. This was not unexpected as exosomes are derived from the endosomal system and play a major role in intercellular communication and immunological function. The plasma exosomal population is frequently increased in the disease state of numerous conditions, including OA, cancer, neurodegenerative diseases, cardiovascular diseases, and COVID-19.[24] Furthermore, these exosomes can contain modified cargo, which not only alters their immunomodulatory capabilities, but also allows them to be targeted as biomarkers of disease. Our findings are in agreement with Mustonen et al,[15] who identified no change in human EV concentration between synovial fluid EVs from healthy and late-stage OA human patients, and Clarke et al,[25] who detected an increase in the number of exosomes after OA-induction surgery in an equine model. Our results suggest that advanced PTOA incites an increase in plasma and synovial fluid exosomal population, which we suspect is due to chronic inflammation; however, this cannot be definitively inferred from our experimental design. Conversely, this could be due to coinciding inflammatory disease processes in horses with PTOA.

There were 67 and 74 miRNAs that were DE in plasma and synovial fluid, respectively, from control horses and horses with PTOA. Bioinformatics analysis was performed to analyze the biological processes and pathways affected by the DE miRNAs and their putative mRNA targets in order to enhance our understanding of the roles of the dysregulated miRNAs in the pathogenesis of PTOA. Several plasma EV DE miRNAs identified in our study, including miR-let7, miR-29, miR-144, and miR-199, and miR-1307, were similarly altered in studies[12,13] evaluating the temporal transcriptomic profile of plasma EVs in an equine model of induced OA. Furthermore, miR-95, miR-149, miR-181, miR-193, miR-195, miR-199, and miR-411 identified in our study were recognized as miRNAs and exosomal miRNAs modified in humans with OA.[26] These miRNAs were ascertained to be involved with apoptosis, cartilage development and remodeling, extracellular matrix homeostasis, and inflammatory response.[26] Beyond these previously reported, we have found additional DE plasma miRNAs associated with PTOA, including miR-1, miR-15, miR-17, miR-19, miR-122, miR-132, miR-143, miR-150, miR-154, miR-185, miR-188, miR-192, miR-204, miR-224, miR-329, miR-652, and miR-3200.

Our study identified synovial fluid EV DE miRNAs, including miR-10, miR-29, miR-34, miR-99, miR-107, miR-126, miR-144, miR-146, miR-215, and miR-486, that were also altered in studies[12,13,27] evaluating the temporal transcriptomic profile of synovial fluid EVs in an equine models of naturally occurring and induced OA. In addition, miR-21, miR-29, miR-34, miR-101, miR-105, miR-127, miR-130, miR-144, miR-146, miR-195, miR-199, miR-411, and miR-486 from our study were recognized as miRNAs

and exosomal miRNAs modified in humans with OA.[26,28] These miRNAs have been linked to apoptosis, cartilage development and remodeling, extracellular matrix homeostasis, inflammatory response, and lipid metabolism.[26] We have found additional synovial fluid EV DE miRNAs associated with PTOA, including miR-15, miR-19, miR-122, miR-132, miR-143, miR-150, miR-154, miR-183, miR-185, miR-192, miR-204, miR-214, miR-224, miR-324, miR-329, miR-338, miR-342, miR-363, miR-483, miR-615, miR-652, miR-744, and miR-3200.

Pathways identified by plasma and synovial fluid EV DE miRNAs with known functions in OA and other similar disease processes included inflammation,[29] proliferation of chondrocytes,[30] and fibrosis.[31] Canonical pathways identified for plasma and synovial fluid have established roles in OA pathogenesis in horses and humans, including apoptosis[32,33]; senescence[34]; fibrosis[31]; TGFβ signaling[35]; inhibitor of DNA binding 1, also known as inductor of differentiation-1 signaling[36,37]; retinoic acid-binding protein activation[38,39]; and peroxisome proliferator-activated receptor/retinoid X receptor activation.[40,41] These enriched top-signaling pathways and canonical pathways observed in both plasma and synovial fluid further support the importance of the role of these DE miRNAs in the biological processes associated with PTOA development.

Predicted targets of plasma and synovial fluid EV DE miRNAs of interest appear to be involved in processes of fibrosis, inflammation, and cellular destruction, including necrosis and apoptosis, which are implicated in the pathogenesis of OA in horses and humans. They act through various mechanisms involving proinflammatory cytokines production,[42,43] synovial inflammation,[43,44] fibroblast proliferation,[45] chondrocyte apoptosis,[32,46] and subchondral bone changes.[47] Many canonical pathways enriched by the plasma and synovial fluid EV DE miRNA putative target genes were essential for or related to PTOA pathogenesis, including the "OA pathway" and "rheumatoid arthritis pathway." Additionally, downstream targets of these signaling pathways with known roles in OA pathogenesis were identified for plasma EVs consisting of matrix MMP3,[48] MMP14,[49] a disintegrin and MMP with thrombospondin motifs 2,[50] and receptor tyrosine-protein kinase (ERBB4).[51] Synovial fluid EV-signaling pathway downstream targets included VEGF,[50] histone deacetylase 4,[52] and specificity protein 1.[53] In our study, fibrosis was the most significant canonical pathway identified from both plasma and synovial fluid EV DE miRNAs and their putative mRNAs targets. Synovial fibrosis is often found in OA,[31,54] which justifies its utility as a grading criterion for the microscopic scoring of OA in horses.[17] Fibrosis is considered a wound-healing process,[31] which was one of the top canonical signaling pathways in our synovial fluid EV DE miRNAs and their putative mRNA targets. Moreover, one of the top upstream regulators in our mRNA target gene analysis in both plasma and synovial fluid EVs was TGFβ, which is a recognized regulator of fibrosis in humans.[55] Our findings shed light on the potential importance of these pathways in PTOA.

In addition to TGFβ, other upstream regulators for both plasma and synovial fluid EVs included miR-16-5p, miR-29b-3p, and miR-146a-5p. The top upstream regulator, miR-16-5p, plays an important role in regulating SMAD3 expression in human chondrocytes in the development of OA.[56] The upstream regulator miR-29b-3p is a known regulator of chondrocyte proliferation and is highly expressed in peripheral blood mononuclear cells and the synovial fluid of humans with OA and identified as a potential biomarker for OA.[57] Lastly, miR-146a-5p has been suggested as a potential biomarker for OA as it was overexpressed in both the serum and cartilage of human patients with OA.[58] This overlap between our findings in horses and the current literature in humans suggests similar molecular processes in the pathogenesis of OA. Equine models of OA have numerous advantages, including similar cartilage and subchondral bone anatomy, gravitational forces, and prevalence of naturally occurring OA.[59,60] They allow for diagnostic imaging, serial synovial fluid collection, arthroscopic intervention, and acquisition of large tissue samples[61,62] in addition to quantifiable, clinically relevant outcomes, such as lameness, joint effusion, and range of motion.[63] Our findings tentatively add support to the utility of the horse as a highly suitable translational animal model to explore the pathogenesis and therapeutic interventions in both veterinary and human OA.

We acknowledge that our study has several limitations. While there was a significant difference in age between the 2 groups, a previous study did not find any differences in synovial fluid–derived EV characteristics or selected miRNA expression between young (0 to 5 years) and old (14 to 21 years) horses.[64] Only 2 cohorts were included in this study, healthy horses and horses with advanced PTOA, as established by macroscopic evaluation. Small noncoding RNA signatures have been evaluated in horses with naturally occurring early-stage OA; however, studies comparing early-stage and late-stage naturally occurring OA are lacking.[27] The future inclusion of different stages of PTOA will provide us with further insight regarding the progression of miRNA dysregulation in these horses. In our study, macroscopic grading was restricted to the radiocarpal, middle carpal, and metacarpophalangeal joints. Samples from the cohort of control horses could have been affected by the undetermined presence of OA in joints that did not undergo gross evaluation. A major restraint was limited sample volume, principally synovial fluid, for use across multiple assays. Isolated EV samples from each group had to be pooled due the low RNA concentration, which prevented us from doing any inferential statistics of our transcriptome analysis. Future studies would benefit from a larger cohort and validating outcomes using additional assays to examine miRNA expression, such as quantitative real-time PCR. Nevertheless, this was the first study to use sRNA sequencing to explore miRNAs profiles in an unbiased manner from healthy horses and horses with PTOA.

In conclusion, our exploratory study demonstrates that equine plasma and synovial fluid EVs display altered miRNA profiles in horses with naturally occurring PTOA when compared to control horses as defined by macroscopic scoring of joint surfaces. Many of the plasma and synovial fluid EV DE miRNAs have previously been demonstrated to have a role in OA. The changing miRNAs and their target genes may play an important role in PTOA pathogenesis by influencing biological cellular processes. This opens the possibility of a relatively noninvasive method, such as blood or synovial fluid sample submission, for early OA detection. Moreover, characterization of these dynamic molecular changes will further elucidate the role of EVs in the pathogenesis of PTOA and bring us a step closer to developing a diagnostic test with adequate sensitivity to surveil disease progression and identify potential therapeutic targets in the signaling pathways. Future studies promise to advance strategies in the prevention and management of PTOA in horses and humans alike.

Disclosures

Dr. Ortved served as guest editor for this JAVMA supplemental issue. She declares that she had no role in the editorial direction of this manuscript. All authors declare that the research was conducted in the absence of any commercial or financial relationships that could be construed as a potential conflict of interest.

All claims expressed in this article are solely those of the authors and do not necessarily represent those of their affiliated organizations or those of the publisher, the editors, and the reviewers. Any product that may be evaluated in this article, or claim that may be made by its manufacturer, is not guaranteed or endorsed by the publisher.

No AI assisted technologies were used in the generation of this manuscript.

References

1. Charalambous CP. The response of articular cartilage to mechanical injury. In: Banaszkiewicz PA, Kader DF, eds. *Classic Papers in Orthopaedics.* London: Springer London, 2014;381–383.

2. Strauss EJ, Goodrich LR, Chen CT, Hidaka C, Nixon AJ. Biochemical and biomechanical properties of lesion and adjacent articular cartilage after chondral defect repair in an equine model. *Am J Sports Med.* 2005;33(11):1647–1653. doi:10.1177/0363546505275487

3. Bertone AL, Ishihara A, Zekas LJ, et al. Evaluation of a single intra-articular injection of autologous protein solution for treatment of osteoarthritis in horses. *Am J Vet Res.* 2014;75(2):141–151. doi:10.2460/ajvr.75.2.141

4. Linardi RL, Dodson ME, Moss KL, King WJ, Ortved KF. The effect of autologous protein solution on the inflammatory Cascade in stimulated equine chondrocytes. *Front Vet Sci* 2019;6:64. doi:10.3389/fvets.2019.00064

5. Ferris DJ, Frisbie DD, Kisiday JD, et al. Clinical outcome after intra-articular administration of bone marrow derived mesenchymal stem cells in 33 horses with stifle injury. *Vet Surg.* 2014;43(3):255–265. doi:10.1111/j.1532-950X.2014.12100.x

6. György B, Szabó TG, Pásztói M, et al. Membrane vesicles, current state-of-the-art: emerging role of extracellular vesicles. *Cell Mol Life Sci.* 2011;68(16):2667–2688. doi:10.1007/s00018-011-0689-3

7. O'Brien TJ, Hollinshead F, Goodrich LR. Extracellular vesicles in the treatment and prevention of osteoarthritis: can horses help us translate this therapy to humans? *Extracell Vesicles Circ Nucl Acids.* 2023;4(2):151–169. doi:10.20517/evcna.2023.11

8. Doyle L, Wang M. Overview of extracellular vesicles, their origin, composition, purpose, and methods for exosome isolation and analysis. *Cells.* 2019;8(7):727. doi:10.3390/cells8070727

9. Isola AL, Chen S. Extracellular vesicles: important players in immune homeostasis. *Ann Transl Med.* 2017;5(suppl 1):S16. doi:10.21037/atm.2017.03.76

10. Withrow J, Murphy C, Liu Y, Hunter M, Fulzele S, Hamrick MW. Extracellular vesicles in the pathogenesis of rheumatoid arthritis and osteoarthritis. *Arthritis Res Ther.* 2016;18(1):286. doi:10.1186/s13075-016-1178-8

11. Kolhe R, Hunter M, Liu S, et al. Gender-specific differential expression of exosomal miRNA in synovial fluid of patients with osteoarthritis. *Sci Rep.* 2017;7(1):2029. doi:10.1038/s41598-017-01905-y

12. Anderson JR, Johnson E, Jenkins R, et al. Multi-omic temporal landscape of plasma and synovial fluid-derived extracellular vesicles using an experimental model of equine osteoarthritis. *Int J Mol Sci.* 2023;24(19):14888. doi:10.3390/ijms241914888

13. Anderson JR, Jacobsen S, Walters M, et al. Small non-coding RNA landscape of extracellular vesicles from a post-traumatic model of equine osteoarthritis. *Front Vet Sci.* 2022;9(901):901269. doi:10.3389/fvets.2022.901269

14. Mustonen AM, Lehmonen N, Paakkonen T, et al. Equine osteoarthritis modifies fatty acid signatures in synovial fluid and its extracellular vesicles. *Arthritis Res Ther.* 2023;25(1):39. doi:10.1186/s13075-023-02998-9

15. Mustonen AM, Lehmonen N, Oikari S, et al. Counts of hyaluronic acid-containing extracellular vesicles decrease in naturally occurring equine osteoarthritis. *Sci Rep.* 2022;12(1):17550. doi:10.1038/s41598-022-21398-8

16. Clarke EJ, Lima C, Anderson JR, et al. Optical photothermal infrared spectroscopy can differentiate equine osteoarthritic plasma extracellular vesicles from healthy controls. *Anal Methods.* 2022;14(37):3661–3670. doi:10.1039/D2AY00779G

17. McIlwraith CW, Frisbie DD, Kawcak CE, Fuller CJ, Hurtig M, Cruz A. The OARSI histopathology initiative – recommendations for histological assessments of osteoarthritis in the horse. *Osteoarthr Cartil.* 2010;18(suppl 3):S93–S105. doi:10.1016/j.joca.2010.05.031

18. Boere J, Van De Lest CHA, Libregts SFWM, et al. Synovial fluid pretreatment with hyaluronidase facilitates isolation of CD44+ extracellular vesicles. *J Extracell Vesicles.* 2016;5:31751. doi:10.3402/jev.v5.31751

19. Chen J, Bardes EE, Aronow BJ, Jegga AG. ToppGene Suite for gene list enrichment analysis and candidate gene prioritization. *Nucleic Acids Res.* 2009;37:W305–W311. doi:10.1093/nar/gkp427

20. Supek F, Bošnjak M, Škunca N, Šmuc T. REVIGO summarizes and visualizes long lists of Gene ontology terms. *PLoS ONE.* 2011;6(7):e21800. doi:10.1371/journal.pone.0021800

21. Shannon P, Markiel A, Ozier O, et al. Cytoscape: a software environment for integrated models of biomolecular interaction networks. *Genome Res.* 2003;13(11):2498–2504. doi:10.1101/gr.1239303

22. Holcar M, Ferdin J, Sitar S, et al. Enrichment of plasma extracellular vesicles for reliable quantification of their size and concentration for biomarker discovery. *Sci Rep.* 2020;10(1):21346. doi:10.1038/s41598-020-78422-y

23. Aae TF, Karlsen TA, Haugen IK, Risberg MA, Lian OB, Brinchmann JE. Evaluating plasma extracellular vesicle microRNAs as possible biomarkers for osteoarthritis. *Osteoarthr Cartil Open.* 2020;1(3-4):100018. doi:10.1016/j.ocarto.2019.100018

24. Mosquera-Heredia MI, Morales LC, Vidal OM, et al. Exosomes: potential disease biomarkers and new therapeutic targets. *Biomedicines.* 2021;9(8):1061. doi:10.3390/biomedicines9081061

25. Clarke EJ, Johnson E, Caamaño Gutierrez E, et al. Temporal extracellular vesicle protein changes following intraarticular treatment with integrin α10β1-selected mesenchymal stem cells in equine osteoarthritis. *Front Vet Sci.* 2022;9:1057667. doi:10.3389/fvets.2022.1057667

26. Mihanfar A, Shakouri SK, Khadem-Ansari MH, et al. Exosomal miRNAs in osteoarthritis. *Mol Biol Rep.* 2020;47(6):4737–4748. doi:10.1007/s11033-020-05443-1

27. Castanheira C, Balaskas P, Falls C, et al. Equine synovial fluid small non-coding RNA signatures in early osteoarthritis. *BMC Vet Res.* 2021;17(1):26. doi:10.1186/s12917-020-02707-7

28. Kharaz YA, Zamboulis DE, Fang Y, Welting TJM, Peffers MJ, Comerford EJ. Small RNA signatures of the anterior cruciate ligament from patients with knee joint osteoarthritis. *Front Mol Biosci.* 2023;10:1266088. doi:10.3389/fmolb.2023.1266088

29. Lieberthal J, Sambamurthy N, Scanzello CR. Inflammation in joint injury and post-traumatic osteoarthritis. *Osteoarthr Cartil.* 2015;23(11):1825–1834. doi:10.1016/j.joca.2015.08.015

30. Liu Y, Zou R, Wang Z, Wen C, Zhang F, Lin F. Exosomal KLF3-AS1 from hMSCs promoted cartilage repair and chondrocyte proliferation in osteoarthritis. *Biochem J.* 2018;475(22):3629–3638. doi:10.1042/BCJ20180675

31. Remst DFG, Blaney Davidson EN, Van Der Kraan PM. Unravelling osteoarthritis-related synovial fibrosis: a step closer to solving joint stiffness. *Rheumatology.* 2015;54(11):1954–1963. doi:10.1093/rheumatology/kev228

32. Hwang H, Kim H. Chondrocyte apoptosis in the pathogenesis of osteoarthritis. *Int J Mol Sci.* 2015;16(11):26035–26054. doi:10.3390/ijms161125943

33. Yang L, Yu X, Liu M, Cao Y. A comprehensive analysis of biomarkers associated with synovitis and chondrocyte apoptosis in osteoarthritis. *Front Immunol.* 2023;14:1149686. doi:10.3389/fimmu.2023.1149686

34. Jeon OH, David N, Campisi J, Elisseeff JH. Senescent cells and osteoarthritis: a painful connection. *J Clin Invest.* 2018;128(4):1229–1237. doi:10.1172/JCI95147

35. Blaney Davidson EN, Van Der Kraan PM, Van Den Berg WB. TGF-β and osteoarthritis. *Osteoarthr Cartil.* 2007;15(6):597–604. doi:10.1016/j.joca.2007.02.005

36. Madej W, van Caam A, Blaney Davidson EN, van der Kraan PM, Buma P. Physiological and excessive mechanical compression of articular cartilage activates Smad2/3P signaling. *Osteoarthr Cartil.* 2014;22(7):1018–1025. doi:10.1016/j.joca.2014.04.024

37. Edhayan G, Ohara RA, Stinson WA, et al. Inflammatory properties of inhibitor of DNA binding 1 secreted by synovial fibroblasts in rheumatoid arthritis. *Arthritis Res Ther.* 2016;18:87. doi:10.1186/s13075-016-0984-3

38. Chiaradia E, Pepe M, Sassi P, et al. Comparative label-free proteomic analysis of equine osteochondrotic chondrocytes. *J Proteomics.* 2020;228:103927. doi:10.1016/j.jprot.2020.103927

39. A Z, Cd K, Ad V, T K, Li S. Expression of retinoic acid receptor (RAR) α protein in the synovial membrane from patients with osteoarthritis and rheumatoid arthritis. *Int J Biomed Sci.* 2007;3(1):46–49.

40. Li XF, Sun YY, Bao J, et al. Functional role of PPAR-γ on the proliferation and migration of fibroblast-like synoviocytes in rheumatoid arthritis. *Sci Rep.* 2017;7(1):12671. doi:10.1038/s41598-017-12570-6

41. Yang H, Wu J-J, Tang T, Liu KD, Dai C. CRISPR/Cas9-mediated genome editing efficiently creates specific mutations at multiple loci using one sgRNA in Brassica napus. *Sci Rep.* 2017;7(1):7489. doi:10.1038/s41598-017-07871-9

42. Goldring SR, Goldring MB. The role of cytokines in cartilage matrix degeneration in osteoarthritis. *Clin Orthop Relat Res.* 2004;427(suppl 427):S27–S36. doi:10.1097/01.blo.0000144854.66565.8f

43. Sutton S, Clutterbuck A, Harris P, et al. The contribution of the synovium, synovial derived inflammatory cytokines and neuropeptides to the pathogenesis of osteoarthritis. *Vet J.* 2009;179(1):10–24. doi:10.1016/j.tvjl.2007.08.013

44. Wang X, Hunter DJ, Jin X, Ding C. The importance of synovial inflammation in osteoarthritis: current evidence from imaging assessments and clinical trials. *Osteoarthr Cartil.* 2018;26(2):165–174. doi:10.1016/j.joca.2017.11.015

45. Scanzello CR, Goldring SR. The role of synovitis in osteoarthritis pathogenesis. *Bone.* 2012;51(2):249–257. doi:10.1016/j.bone.2012.02.012

46. Thomas CM, Fuller CJ, Whittles CE, Sharif M. Chondrocyte death by apoptosis is associated with cartilage matrix degradation. *Osteoarthr Cartil.* 2007;15(1):27–34. doi:10.1016/j.joca.2006.06.012

47. Stewart HL, Kawcak CE. The importance of subchondral bone in the pathophysiology of osteoarthritis. *Front Vet Sci.* 2018;5:178. doi:10.3389/fvets.2018.00178

48. Burrage PS, Mix KS, Brinkerhoff CE. Matrix metalloproteinases: role in arthritis. *Front Biosci.* 2006;11:529–543. doi:10.2741/1817

49. Wang G, Chen S, Xie Z, et al. TGFβ attenuates cartilage extracellular matrix degradation via enhancing FBXO6-mediated MMP14 ubiquitination. *Ann Rheum Dis.* 2020;79(8):1111–1120. doi:10.1136/annrheumdis-2019-216911

50. Turlo AJ, McDermott BT, Barr ED, et al. Gene expression analysis of subchondral bone, cartilage, and synovium in naturally occurring equine palmar/plantar osteochondral disease. *J Orthop Res.* 2022;40(3):595–603. doi:10.1002/jor.25075

51. Wang Z, Bao H, Hou J, Ju B, Ji Y. Circ-NFKB1 sponges miR-203a-5p to regulate ERBB4 expression and promotes IL-1β induced chondrocytes apoptosis. *J Orthop Surg Res.* 2023;18(1):528. doi:10.1186/s13018-023-03990-4

52. Lu J, Sun Y, Ge Q, Teng H, Jiang Q. Histone deacetylase 4 alters cartilage homeostasis in human osteoarthritis. *BMC Musculoskelet Disord.* 2014;15:438. doi:10.1186/1471-2474-15-438

53. He W, Lin X, Chen K. Specificity protein 1-mediated ACSL4 transcription promoted the osteoarthritis progression through suppressing the ferroptosis of chondrocytes. *J Orthop Surg Res.* 2023;18(1):188. doi:10.1186/s13018-023-03673-0

54. Rim YA, Ju JH. The role of fibrosis in osteoarthritis progression. *Life.* 2020;11(1):3. doi:10.3390/life11010003

55. Zhong L, Huang X, Karperien M, Post JN. Correlation between gene expression and osteoarthritis progression

in human. *Int J Mol Sci.* 2016;17:1126. doi:10.3390/ijms17071126

56. Li L, Jia J, Liu X, et al. MicroRNA-16-5p controls development of osteoarthritis by targeting SMAD3 in chondrocytes. *Curr Pharm Des.* 2015;21(35):5160–5167. doi:10.2174/1381612821666150909094712

57. Chen C, Chen H. Clinical diagnosis value of miR-29b-3p in peripheral blood mononuclear cells and synovial fluid among osteoarthritis patients. *Clin Lab.* 2019;65(8). doi:10.7754/Clin.Lab.2019.190139

58. Skrzypa M, Szala D, Gablo N, et al. miRNA-146a-5p is upregulated in serum and cartilage samples of patients with osteoarthritis. *Pol Przegl Chir.* 2019;91(3):1–5. doi:10.5604/01.3001.0013.0135

59. Frisbie DD, Cross MW, McIlwraith CW. A comparative study of articular cartilage thickness in the stifle of animal species used in human pre-clinical studies compared to articular cartilage thickness in the human knee. *Vet Comp Orthop Traumatol.* 2006;19(3):142–146. doi:10.1055/s-0038-1632990

60. McIlwraith CW, Frisbie DD, Kawcak CE. The horse as a model of naturally occurring osteoarthritis. *Bone Joint Res.* 2012;1(11):297–309. doi:10.1302/2046-3758.111.2000132

61. Bertoni L, Jacquet-Guibon S, Branly T, et al. An experimentally induced osteoarthritis model in horses performed on both metacarpophalangeal and metatarsophalangeal joints: technical, clinical, imaging, biochemical, macroscopic and microscopic characterization. *PLoS ONE.* 2020;15(6):e0235251. doi:10.1371/journal.pone.0235251

62. Frisbie D, Ghivizzani S, Robbins P, Evans CH, McIlwraith CW. Treatment of experimental equine osteoarthritis by in vivo delivery of the equine interleukin-1 receptor antagonist gene. *Gene Ther.* 2002;9(1):12–20. doi:10.1038/sj.gt.3301608

63. Cook JL, Hung CT, Kuroki K, et al. Animal models of cartilage repair. *Bone Joint Res.* 2014;3(4):89–94. doi:10.1302/2046-3758.34.2000238

64. Addis A, Clarke EJ, Peffers MJ. Characterisation of Equine Synovial Fluid Derived Extracellular Vesicles from Young and Old Horses. 2022. Accessed January 29, 2024. https://livrepository.liverpool.ac.uk/id/eprint/3150605

Supplementary Materials

Supplementary materials are posted online at the journal website: avmajournals.avma.org